Scanning Microscopy

Volume 1 | Number 2 Article 10

2-6-1987

Theory of Electron Beam Induced Current and Cathodoluminescence Contrasts from Structural Defects of Semiconductor Crystals; Steady-State and Time-Resolved Problems

A. Jakubowicz
Max-Planck-Institut für Festkörperforschung

Scanning Microscopy, Vol. 1, No. 2, 1987 (Pages 515-533)
Scanning Microscopy International, Chicago (AMF O'Hare), IL 60666 USA

0891-7035/87$3.00+.00

THEORY OF ELECTRON BEAM INDUCED CURRENT AND CATHODOLUMINESCENCE CONTRASTS FROM STRUCTURAL DEFECTS OF SEMICONDUCTOR CRYSTALS; STEADY-STATE AND TIME-RESOLVED PROBLEMS

A. Jakubowicz*

Max-Planck-Institut für Festkörperforschung, Heisenbergstr. 1, D-7000 Stuttgart 80,
Federal Republic of Germany
*On leave from the Institute of Electron Technology, Technical University of Wroclaw,
ul. Janiszewskiego 11/17, 50-372 Wroclaw,
Poland

(Received for publication April 10, 1986, and in revised form February 06, 1987)

Abstract

Electron-beam-induced current and cathodoluminescence are powerful tools for revealing and characterizing point-like defects, dislocations, and grain boundaries in semiconductor crystals.

This paper reviews the theoretical studies of electron-beam-induced current and cathodoluminescence contrasts from local structure defects of semiconductor crystals (the geometrical aspects of both contrasts, the assessment of the defect properties from the contrast, the evaluation of bulk parameters in the presence of defects, and time-resolved characterization of defects), including recent developments in this area.

KEY WORDS: Scanning electron microscopy, electron-beam-induced current, cathodoluminescence, contrast, defects, dislocations, grain-boundaries, time-resolved measurements.

*Address for correspondence:
A. Jakubowicz
Max-Planck-Institut für Festkörperforschung
Heisenbergstr. 1, D-7000 Stuttgart 80
Federal Republic of Germany
Phone No. (0711) 6860379

Introduction

The properties of semiconductor crystalline materials and devices depend strongly on the presence of electrically active defects in the materials. This implies the necessity of using special diagnostic methods which allow to detect and characterize such defects. Among SEM techniques charge collection microscopy (CCM) and cathodoluminescence (CL) have proven to be powerful tools for the investigation of material imperfections. Both techniques have been reviewed recently: CCM - by Leamy [42] and Holt and Lesniak [28], and CL - by Holt and Saba [29] and Yacobi and Holt [78].

Charge Collection Microscopy - Principles of Contrast Formation

The SEM electron beam produces a quantity of electron-hole pairs in a semiconducting specimen. To detect them an electrical barrier (Schottky contact, p-n junction) is used (Fig. 1a and b). These carriers which are produced inside the electric field region of the barrier, and those which reach this region by diffusion, are separated giving rise to an electrical signal in the external circuit. A detailed theoretical analysis of the injected carrier transport, with steady-state and time-dependent solutions, has been performed by van Roosbroeck [72]. Material imperfections of electrical nature are detected by measurement of variations in collected charge as a function of beam position. In this paper, only defects located outside the electrical field region of the collecting barrier are discussed. The barrier is assumed to be "ideal", i.e. such phenomena as microplasma formation [28] or barrier thickness and electrical field modulation [41] are not taken into account.

Both methods shown schematically in Fig. 1a and b presume the presence of a separate barrier. However, some defects can be detected by using for charge collection their own space charge regions (see Detection of Space Charge Regions).

The mechanism of contrast formation is presented schematically for a point-like defect (Fig. 1c). Since the collected current is proportional to the local recombination (sometimes also generation) rate for electron-hole pairs, one obtains a reduced signal when the beam comes close to a defect acting as a system of recom-

bination centres. On the contrary, an enhanced signal is observed when the imperfection acts as a region of reduced recombination. It is convenient to use the concept of the contrast profile [16]

$$c(x,y) = \frac{I_0 - I_d(x,y)}{I_0} \qquad (1)^*$$

where $c(x,y)$ is the contrast profile, and I_0 and $I_d(x,y)$ are signals measured when the beam is located infinitely far from the defect, and at a distance $(x^2+y^2)^{1/2}$ (see Fig. 1c), respectively. Usually the signals are short circuit currents (hence the popular name of the method: EBIC ≡ electron-beam-induced current). Thus the theoretical problem is to calculate the total current collected by a Schottky contact or p-n junction as a function of the position of the electron

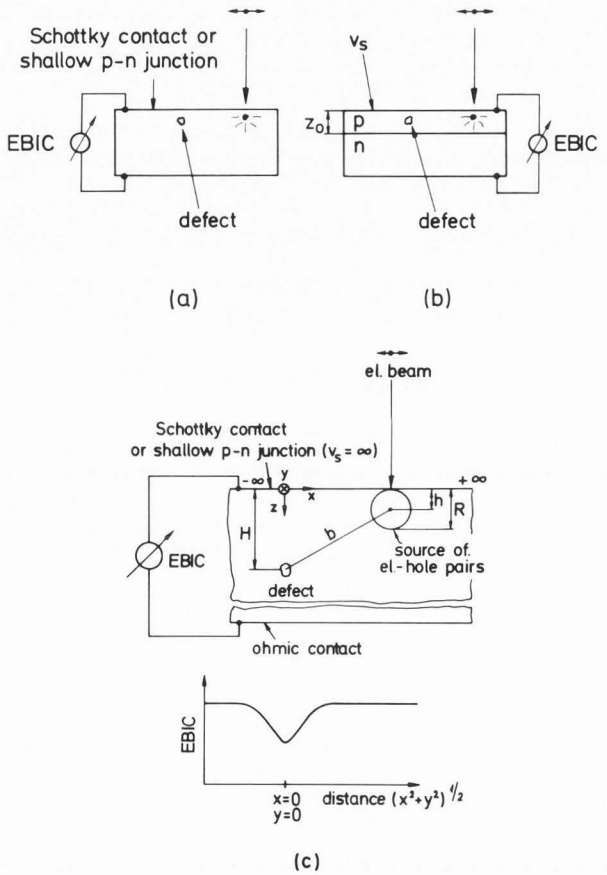

Fig. 1. Standard geometries used for CCM investigations of defects; the carriers are collected by a (a) Schottky contact or shallow p-n junction, (b) p-n junction at depth z_0, (c) schematic illustration of contrast formation for the structure (a). The thickness of the sample is assumed to be much greater than the minority carrier diffusion length.

*See List of Symbols at the end of the paper.

beam relative to the defect. This can be done by using the general formula

$$I = qD \int_P \left. \frac{\partial \delta n(\bar{r})}{\partial z} \right|_{z=z_0} dP \qquad (2)$$

where q is the magnitude of electronic charge, D is the minority carrier diffusion coefficient, P is the area of the collecting barrier, $\delta n(\bar{r})$ is the density of excess minority carriers with $\bar{r}$ representing the coordinates in three dimensions, and z_0 is the depth of the collecting barrier. The density $\delta n(\bar{r})$ obeys the continuity equation

$$D\nabla^2 \delta n(\bar{r}) - \frac{1}{\tau(\bar{r})} \delta n(\bar{r}) + g(\bar{r}) = 0 \qquad (3)$$

where $\tau(\bar{r})$ is the lifetime of minority carriers, and $g(\bar{r})$ is the number of generated electron-hole pairs per unit time and volume. The collecting barrier is usually assumed to be a plane characterized by a recombination velocity $v_s = \infty$, i.e. one assumes the barrier to be a sink for minority carriers of infinite strength. The appropriate boundary condition is $\delta n = 0$. For the structure from Fig. 1b one needs an additional boundary condition at the surface: $D(\partial\delta n/\partial z) = v_s \delta n$. In the particular case $v_s = \infty$ one has again $\delta n = 0$.

Different approaches have been used for introducing the defect into the theoretical analysis. The choice of a quantity describing the defect depends on its geometry and its specific character. For example in polycrystalline solar cells it is reasonable to idealize grain boundaries by planes having an effective minority carrier recombination velocity (by analogy to the surface recombination velocity), whereas in studies of minority carrier recombination at dislocations it is reasonable to replace the dislocation by a cylinder of an effective capture radius r_{eff} with $\delta n = 0$ at the cylindrical surface. Briefly summarizing the approaches usually used in theoretical studies of EBIC contrast: point-like defects (for example impurity clusters) and line defects (dislocations) have been treated as regions of a reduced minority carrier lifetime (diffusion length) or characterized by an effective capture radius, planar defects (grain boundaries) have been described by an effective minority carrier recombination velocity, and extended defects of more complex shapes have been regarded as consisting of the elementary defects mentioned above.

An important quantity which must be defined for theoretical calculations of the contrast is the function $g(\bar{r})$ describing the distribution of the generated electron-hole pairs. Again, the choice of $g(\bar{r})$ depends on the considered problem. It is enough to assume a point source when the electron beam comes not to close to the defect or when the source is small enough. Otherwise an extended source should be taken into account. Although the actual form of $g(\bar{r})$ is known, for mathematical convenience different approximate representations of $g(\bar{r})$ are used, depending on the problem being considered. Many authors assumed the source to be a sphere of finite dimensions with $g(\bar{r})$ being constant (for example see Ref. 16,45). For accurate quantitative evalua-

tions it may be necessary to consider a more realistic source (for example a Gaussian source [21]).

EBIC Contrast of Point-Like Defects and Dislocations

It is convenient to discuss the models for point-like defects and dislocations together, since in many theoretical studies both types of defects have been treated in a similar way. A simple expression for the contrast has been proposed by Ioannou and Davidson [31]. Assuming an ideal steady-state point source located at a distance h beneath the surface of a semi-infinite sample (Fig. 1c) and taking

$$I_0 = q\, g_0 \exp(-h/L) \qquad (4)$$

where L is the minority carrier diffusion length, and g_0 the generation rate, they found by differentiating equation (4)

$$c = \frac{h}{L}\,\frac{\Delta L}{L} \qquad (5)$$

where ΔL is the local reduction of L.
A similar approach for the geometry from Fig. 1b yields [31]

$$c = \frac{z_0^2 - h^2}{L^2}\,\frac{\Delta L}{L} \qquad (6)$$

where z_0 is the p-n junction depth. These expressions predicted correctly the observed dependence of the contrast on the beam energy (the electron penetration depth was calculated by using the model of Kanaya and Okayama [37]. The applicability of equations (5) and (6) is strongly limited since they do not predict full contrast profiles. There is no information about the depth of the defect and its geometry. Full contrast profiles have been calculated by Donolato [16]. He assumed the defect to be a bounded region, where the minority carrier lifetime τ_d was lower than in the rest of the semiconductor. From a modified continuity equation

$$D\nabla^2\,\delta n(\bar{r}) - \frac{1}{\tau}\,\delta n(\bar{r}) = -g(\bar{r}) + \left[\frac{1}{\tau_d(\bar{r})} - \frac{1}{\tau}\right] e(\bar{r})\,\delta n(\bar{r}) \qquad (7)$$

with τ being the lifetime in the unperturbed bulk, and

$$e(\bar{r}) = \begin{cases} 1 & \text{for } \bar{r} \text{ inside the defect} \\ 0 & \text{elsewhere} \end{cases}$$

he derived the density of the excess minority carriers in a first-order approximation, i.e. the defect was treated as a small perturbation. For the geometry from Fig. 1c, assuming a point defect, and a uniform generation sphere tangent to the surface (an approximation frequently used for silicon) he obtained a relation of the type

$$c = \gamma_d\, f(b,R,H,L) \qquad (8)$$

where $\gamma_d = \frac{1}{D}\left(\frac{1}{\tau_d} - \frac{1}{\tau}\right)$ is the "defect strength", b is the distance between the source and the defect, R is the primary electron range, and H is the depth of the defect. Equation (8) says that the contrast is a linear function of the defect strength. The function f(b,R,H,L) describes the geometrical aspects of the contrast (b,R,H) and characterizes the recombination properties of the material (L). For realistic values H = 2 μm, L = 10 μm, and for typical R values between 0.8 μm to 10 μm (for silicon) Donolato has obtained from equation (8) the contrast profiles reported in Fig. 2. Donolato's model allows to determine two

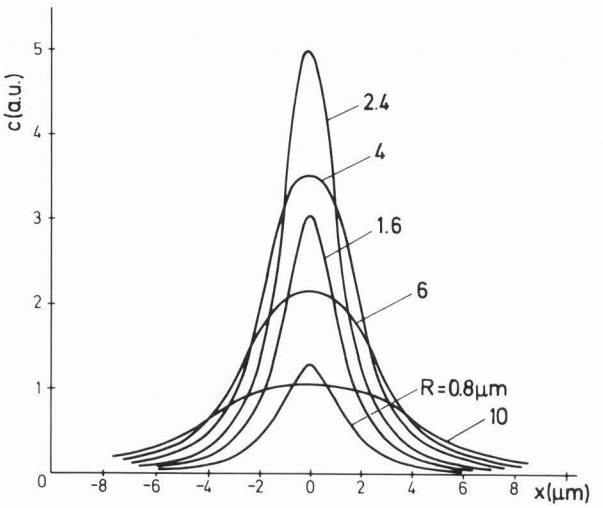

Fig. 2. Calculated contrast profiles for different primary electron ranges R for a point defect at a depth H = 2 μm, and bulk diffusion length L = 10 μm; the defect and the center of the excited volume are in the plane y = 0 (Fig. 2 in Ref. 16).

important relations: a) the contrast magnitude and b) the resolution of the image defined by its half-width w, as a function of the electron beam energy and depth of the defect (Fig. 3). One can see in Fig. 3 that the beam energy that gives the greatest contrast will also give, to a good approximation, the best resolution. The curves in Fig. 3 have been calculated for L = ∞. It follows from Fig. 3 that the spatial resolution of SEM-EBIC images of defects is not limited by the minority carrier diffusion length. The last property can be explained by the three dimensional nature of the minority carrier diffusion. For a small localized defect the resolution is limited by the defect depth or the extension of the generation region, whichever is the greatest [17].

The linear character of Donolato's model allows to use the point defect solution for treating extended defects as a sum of elementary point defect contributions [18]. Assuming, for example, that dislocations are represented as

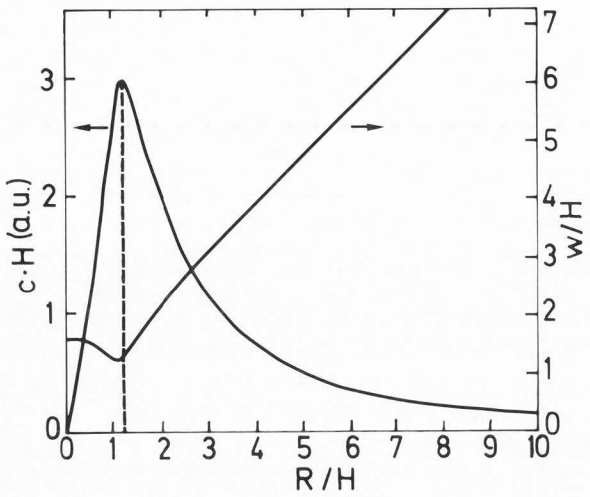

Fig. 3. Contrast and resolution of the image of a point defect versus normalized electron range for the limit case of L = ∞ (Fig. 3 in Ref. 16).

continuous distributions of point defects one finds for a dislocation perpendicular to the surface (using the geometry from Fig. 1c) that the image width of the dislocation is of the order of the electron range R, even for very large values of L, which agrees with experimental findings [18]. Fig. 4a shows this result for silicon. The contrast magnitude calculated for various electron ranges and diffusion lengths is shown in Fig. 4b. The different contrast behavior of a perpendicular dislocation and a small localized defect (compare Figs. 3 and 4b) gives a practical method for establishing whether an image feature corresponds to a dislocation or to a subsurface localized defect [18]. Theoretical calculations of dislocation contrast profiles were performed by several authors. The aim was to find solutions for different geometrical configurations important in practical situations [18,23,20,22,4,39, 56-59,3,9,36]. A general formula for treating a dislocation in both geometries from Fig. 1 has the form [24]

$$c = \gamma \left[\frac{1}{I_0} \int_Y \delta n_0(\vec{r})\ \Phi(z)\ dY\right] \qquad (9)$$

here $\gamma = \pi \ell^2/\tau_d$ (ℓ is the radius of the dislocation), $\delta n_0(\vec{r})$ is the unperturbed distribution of excess minority carriers (for the first order approximation: $\delta n(\vec{r}) \approx \delta n_0(\vec{r})$), $\Phi(z)$ is the carrier collection probability (for the geometry from Fig. 1c, for instance, $\Phi(z) = \exp(-z/L)$), and Y is the length of the dislocation.

Donolato, considering a dislocation parallel to the surface for the structure from Fig. 1b, observed a strong influence of the surface recombination velocity v_s on both the contrast magnitude and the resolution [20]. A low value of v_s generally enhances the contrast, but reduces the resolution. In thin samples, as used for combined SEM/TEM observations, both surface recombination velocity and thickness influence the contrast and the image width [20]. In such samples bulk recombination, and at high beam energies also the lateral spread of the beam, can be neglected. Better resolution is therefore expected for smaller thicknesses and higher values of the surface recombination velocity. The image contrast increases for smaller sample thicknesses and lower surface recombination velocities.

Contrast profiles for inclined dislocations were calculated in Refs. [23,39,3,36]. Beer et al. [3] presented contours of equal contrast for dislocations. In Fig. 5 such contours are given for a dislocation in Si, having an inclination angle 20°. Good agreement with experimental contours was obtained by assuming that the contrast geometry is merely a function of the minimum distance b_{min} between the excitation volume center and the dislocation line (see Fig. 5). Con-

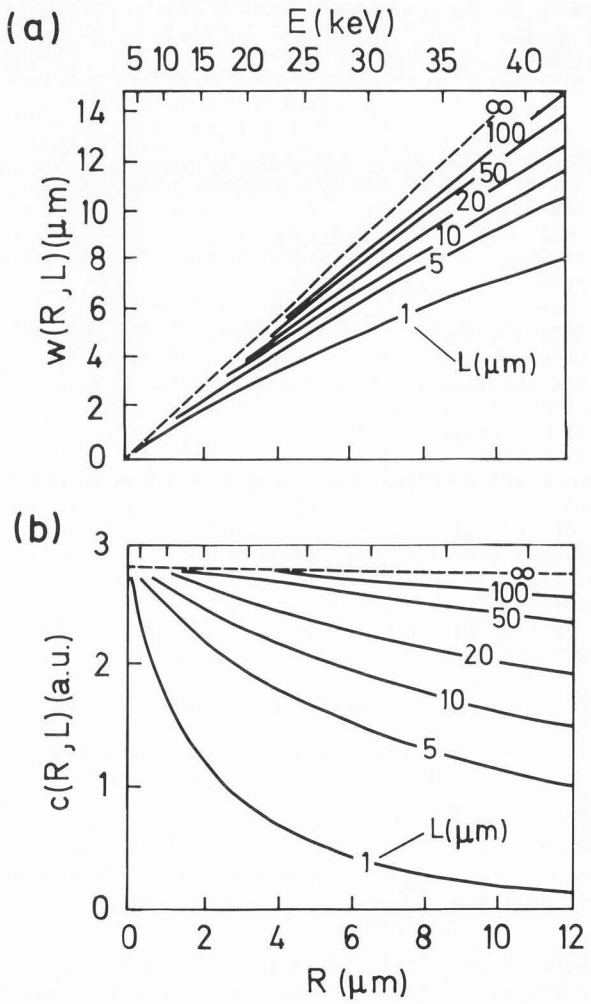

Fig. 4. (a) Resolution and (b) contrast of the EBIC image of a straight dislocation perpendicular to the surface versus electron range for different values of bulk diffusion length. The upper horizontal axes give the corresponding beam energies for silicon (Fig. 2 in Ref. 18).

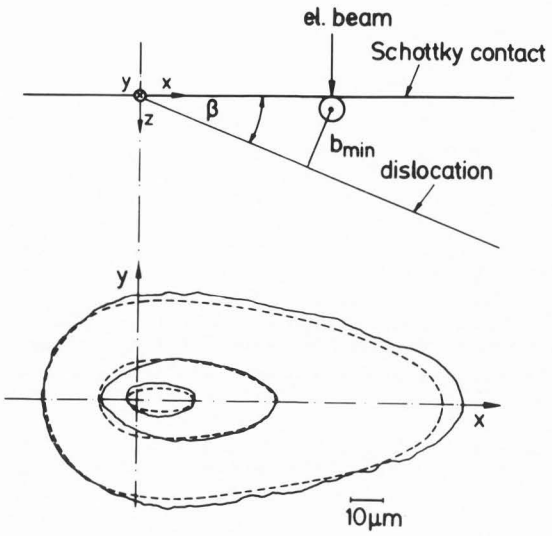

Fig. 5. Experimental and calculated (dashed lines) EBIC contrast contours of a dislocation in Si having an inclination angle $\beta = 20°$ with respect to the surface; L = 30 μm. The upper part of the figure is a schematic representation of the geometry used for calculations; b_{min} is the minimum distance between the center of the source and the dislocation (the contrast contours are from Fig. 4 in Ref. 3).

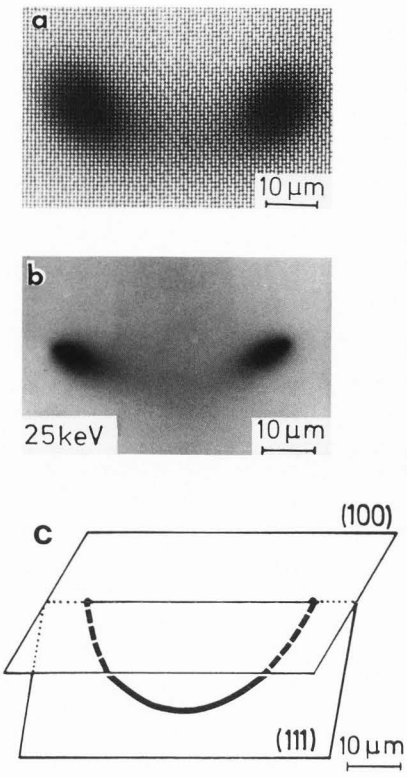

Fig. 6. (a) computer simulated and (b) experimental (at beam energy 25 keV) EBIC images of an oxidation induced stacking fault in (100) Si, (c) schematic representation of the stacking fault (Courtesy of C. Donolato and H. Klann, see Ref. 19).

tour mapping gives a good impression on geometrical features and the range of activity of crystal defects. The approach of Beer et al. does not result in a new contrast model, alternative to that of Donolato. It only uses a geometrical hypothesis which allows to obtain a good fit to experimental contours. A good fit, however, seems also to be possible by taking into account the effects due to the depleted layer of the collecting barrier [23]. In addition, such an approach would have an important advantage; it would reflect better the realistic situation.

Computer simulation yields a method for gaining accurate information on the shape and depth of defects having more complex forms. Halftone SEM-EBIC images have been produced by computer simulation for dislocations and stacking faults [19]. Figs. 6a and b show a simulated image and a Schottky barrier image, respectively, of an oxidation induced stacking fault in (100) Si. The contrast arises from the bounding partial dislocation shown in Fig. 6c. It is conceivable that on-line computer processing of EBIC images at different beam energies will allow to obtain the "electrical shape" of defects with unknown structure.

Sensitivity of EBIC

Donolato's model, which regards the defect as a small perturbation, yields an expression for the contrast, which has generally the form

$$c = \Gamma F \text{ (R,L, geometry)} \qquad (10)$$

with Γ being the strength of a point-like or line defect, and F being rather a complex function which describes the material properties (L), the source (R) and the geometry of the system. For point-like defects one has [39,40]

$$\Gamma_p = \ell^3 \left(\frac{1}{L_d^2} - \frac{1}{L^2}\right) \qquad (11)$$

with ℓ being the dimension of the defect. If $L_d \ll L$ the defect strength is mainly determined by the recombination properties of the defect (L_d) and the defect volume (ℓ^3). For line-shaped defects regarded as pipes with small diameter the defect strength [39,40]

$$\Gamma_\ell = \ell^2 \left(\frac{1}{L_d^2} - \frac{1}{L^2}\right) \qquad (12)$$

is proportional to cross-section ℓ^2.

For the interpretation of EBIC contrasts it is important to estimate the sensitivity of the EBIC technique. There is, for example, evidence that dislocations with impurity atmospheres show much stronger contrast than "clean" dislocations [39]. An estimation of the sensitivity of the EBIC method has been done by assuming the defect to consist of statistically distributed non-interacting recombination centres. Combining equations (10)-(12) with the known relations $L_d = (\tau_d D)^{1/2}$ and $\tau_d = (N_d \sigma_d \nu_{th})^{-1}$ (N_d is the density of recombination centres, σ_d is their capture cross-section, and ν_{th} is the thermal velocity of the minority carriers), and taking $L_d \ll L$ (to estimate the maximum sensitivity) one obtains the minimal detectable number of centres for the

point-like defect $n_{d,min}$ and the minimal detectable line density for line-shaped defects $e_{d,min}$ [39]

$$n_{d,min} \text{ , } e_{d,min} = \frac{c_{min}}{F_{opt}} \frac{D}{\nu_{th} \sigma_d} \qquad (13)$$

where F_{opt} is the appropriate geometrical factor selected for optimum imaging conditions, and c_{min} is the minimum contrast still detectable. c_{min} depends on the signal/noise ratio and for a standard EBIC circuitry has a value $c_{min} \approx 5 \times 10^{-3}$ [39]. From equation (13) it has been found that the detection limit for a cluster of such impurities like Au and Cu in Si ($\sigma_d \approx 10^{-14} cm^2$) amounts to a few hundred atoms [39]. For "clean" dislocations, by interpreting the recombination centres as dangling bonds ($\sigma_d \approx 10^{-16} cm^2$) one needs a line density $e_{d,min} \approx 2 \times 10^4 \mu m^{-1}$ to be detected [39]. Since the expected maximal line density of dangling bonds is $e_d \leq 5 \times 10^3 \mu m^{-1}$, "clean" dislocations may be difficult to detect. For decorated dislocations even a small content of deep impurity centres is sufficient to make the dislocation detectable.

Non-Linear Behavior of EBIC Contrast

To examine the accuracy of the first-order approximation model of Donolato [16] Pasemann performed calculations of the correction due to higher order approximations [56,59,58] (the first-order approximation does not take into account the reduction of the original excess minority carrier density around the defect). He has shown the contrast of a dislocation parallel to the collecting plane to have the form [56]

$$c_k = c_1/(1+k) \qquad (14)$$

where c_1 is the first-order approximation, and k is a non-linear contribution to the contrast depending on: a) the geometry of the sample, b) the surface recombination velocity, c) the position of the dislocation in the sample, and d) the type of the dislocation. One can preserve the "first-order approximation notation" given by equation (9), by introducing a corrected effective recombination strength γ_{eff} of the defect [24]. The relative error of the first-order approximation, equal to k, does not exceed 100%. It is smaller for weaker defects, and for defects located close to a boundary with a high recombination velocity (for example to the collecting barrier). The latter is a consequence of the fact that an absorbing boundary weakens the sink action of the defect.

The main result of Pasemann's calculation is the non-linear behavior of the EBIC contrast related to the parameter which characterizes directly the recombination activity of the defect. The contrast is no longer a product of two "pure" factors: the one describing only the recombination activity of the defect, and the other one which describes the geometry only, as it is predicted by Donolato's model [16]. It may be, therefore, difficult to interpret an EBIC experiment with a non-constant defect strength. Imagine two defects having identical recombination properties but different geometrical positions. Applying the linear relation (10) one can eliminate the geometric factor by normalizing the contrast

$$c_{norm} = \frac{c}{c_0} = \frac{\Gamma}{\Gamma_0} \qquad (15)$$

and thus making the contrast function [$c_{norm} = f(\Gamma)$] identical for both defects. In the non-linear case the normalized contrast still depends on the geometric factor, and will therefore be different for both defects. In fact, EBIC contrast vs temperature measurements performed for individual dislocations in Si have shown that different dislocations of the same type may have different temperature characteristics [55,60,27].

A non-linear model which assumes a different definition of the defect has been developed by Jakubowicz [32]. An EBIC experiment detects a decrease of the current when the beam comes close to the defect. For a point-like defect or a dislocation the strength of the defect sink action depends on a) the radius of the defect, b) the density of recombination centres, c) the character of the recombination process, d) the charge state of the defect, and e) the velocity of carriers. Two defects differing in these parameters may still act as a sink of the same strength, when an appropriate combination of a-e remains constant. Hence it is reasonable to describe the defect by one quantity: an effective capture radius r_{eff}. For a dislocation, for example (Fig. 7a), r_{eff} will be the radius of an actually non-

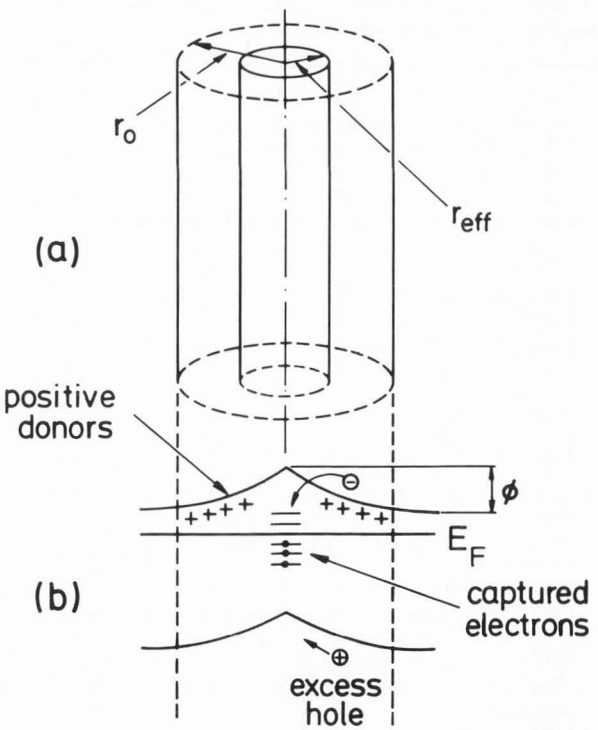

Fig. 7. (a) Schematic representation of a dislocation of radius r_0, and the equivalent dislocation characterized by an effective capture radius r_{eff}, (b) band diagram of a negatively charged dislocation in n-type material; E_F is the Fermi energy and ϕ is the barrier height.

existent cylindrical surface absorbing all excess minority carriers. In fact there is no sharp boundary between the dislocation and the matrix. The sink action of a dislocation begins by attracting minority carriers due to the charge of the dislocation (Fig. 7b), and is then followed by their recombination at the dislocation recombination centres. For an elementary point-like defect problem and the geometry from Fig. 1c Jakubowicz obtained [32]

$$c = f_1(r_{eff},b,h,H,L)\ f_2(b,h,H,L) \quad . \qquad (16a)$$

f_1 is a non-linear function of r_{eff}. As shown in [32] for small capture radii f_1 reduces to a very simple form

$$f_1 = \frac{r_{eff}}{L}\, e^{\frac{r_{eff}}{L}} \quad . \qquad (16b)$$

f_1 shows explicitly the non-linear dependence of the contrast on r_{eff}. The function f_2, describing the geometrical aspects of the contrast, is identical with the one resulting from Donolato's first-order approximation calculations [16]. Thus the essential conclusions of the linear contrast model concerning the geometrical form of the defect, its position in the bulk, and also some recombination properties are preserved with quantitative corrections due to the geometrical parameters involved in f_1 (see eq. 16a). On the other hand the strong non- linear dependence on r_{eff}, and the presence of geometrical parameters in f_1, explain the results of EBIC contrast vs temperature measurements [55].

Jakubowicz's model suggests the possibility to deduce from EBIC measurements directly the capture radius, which is the parameter usually used to characterize defects, and consequently the recombination efficiency of defects [14].

Within the framework of Jakubowicz's model one cannot treat strictly the inside of the defect. However, if the size of the defect is much less than the size of the region excited by the beam one can safely neglect the fraction of carriers generated inside the defect region. For larger defects, but still less than the excited volume, one can improve the accuracy by introducing a fitting parameter describing which effective portion of carriers, generated inside the defect, contributes to the signal.

Non-linear models may provide difficulties in treating exactly defects having complex shapes. In a linear model the integral effect of the defect is simply the sum of elementary, for example point-like, contributions over the whole volume of the defect. The situation complicates if a non-linear approach is applied. Appropriate approximations may then become necessary (see for example [32,36]).

Characterization of Recombination Processes at Individual Dislocations

EBIC offers a possibility of a detailed characterization of the recombination processes at a defect by measuring the variation of the contrast as a function of a parameter which determines the defect capture radius. Kimerling et al. [38], Ourmazd and Booker [53,54], and Cheng [10] have shown that from EBIC contrast versus temperature measurements one can deduce the position of the defect energy level. Ourmazd [54] developed a theoretical model relating the contrast of an individual dislocation to the temperature by assuming a two stage recombination process. For an edge dislocation in heavily doped Si he estimated from the plot $\ln c = f(1/T)$ the activation energy for a shallow energy level in the band gap, involved in recombination. From the slope of $\ln c = f(1/T)$ at low temperatures he was able to deduce the charge state of the dislocation.

EBIC Contrast of Grain Boundaries

A possibility of modeling a grain boundary for EBIC investigations is to regard it as a region of a reduced minority carrier diffusion length. von Roos assumed the diffusion length to be dependent on the distance from the grain boundary as [70]

$$L_x = \frac{x}{\left[\left(\frac{x}{L}\right)^2 + p(p-1)\right]^{1/2}} \qquad (17)$$

with p being an adjustable parameter. Equation (17) signifies a decreasing diffusion length toward the grain boundary. The particular choice for L_x was dictated by the fact that the diffusion equation could be solved in closed form. This model seems impracticable since it uses a non-physical quantity (p), and is very intricate. It is also not applicable when the grain boundary is an abrupt transition between adjacent grains (within several atomic layers). On the other hand, modeling of grain boundaries by an appropriate function L(x) seems reasonable when they are surrounded by clouds of point defects, dislocations and/or denuded zones.

A grain boundary represented as a two-dimensional surface of recombination centers perpendicular to the collection plane was treated by Marek [45] and Dimitriadis [15]. The influence of the grain boundary on the minority carrier distribution was considered as a perturbation. Marek used the point-like defect solution [16], and by a numerical two-dimensional integration he obtained EBIC contrast profiles. Fig. 8 shows the maximum contrast as a function of the beam energy, calculated for a homogeneous generation sphere, touching the surface of a semi-infinite silicon sample. As the generation sphere increases, the carriers have to diffuse over larger distances to be collected at the surface. Therefore the probability of recombining at the grain boundary becomes larger. The same explanation holds for the contrast increase with increasing diffusion length. The situation changes for small diffusion lengths. Now the grain boundary absorbs carriers only from its close vicinity. Thus, with the increase of the generation sphere the fraction of carriers which does not recombine at the grain boundary increases, and the resulting contrast reduces. The maximum contrast for a given diffusion length appears roughly when the diffusion length equals the radius of the generation sphere. Since the contrast profiles show a strong dependence on the diffusion length of the adjacent grains, the latter can be measured through linescans perpendicular to the grain boundary.

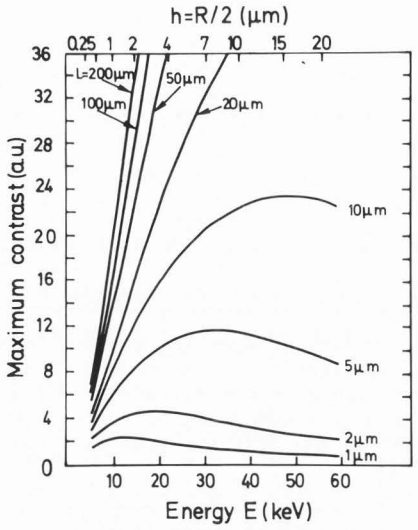

Fig. 8. Calculated maximum contrast of a semi-infinite grain boundary normal to the x axis, for diffusion lengths between 1 μm and 200 μm, and a homogeneous generation sphere touching the surface of a semi-infinite silicon sample (Fig. 3 in Ref. 45).

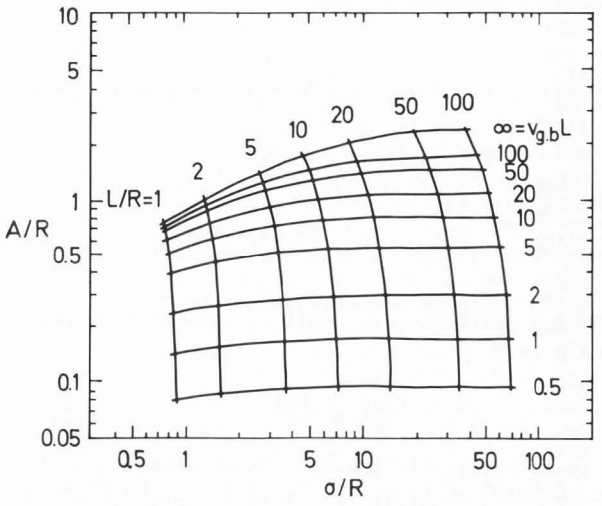

Fig. 9. Diagram relating area and standard deviation of EBIC contrast profile of a grain boundary to the interface recombination velocity $v_{g.b.}$ and bulk diffusion length (Fig.5 in Ref. 25).

Marek [45] proposed the determination of L from the half width of contrast profiles.

A simple analytical expression for the contrast, assuming large diffusion lengths (L >> h), has been derived recently by Dimitriadis [15]. For large enough distances x ≥ L

$$c = 1 - \frac{1}{2\sqrt{2}\pi} \frac{v_{g.b.} L^{1/2}}{D} h \, e^{\frac{h}{L}} \frac{e^{-\frac{x}{L}}}{x^{1/2}} \qquad (18)$$

where $v_{g.b.}$ [cm s^{-1}] is the recombination velocity at the grain boundary. Equation (18) can be used to a quick determination of L from the plot of $\ln[(1-c)x^{1/2}]$ versus x, being a straight line (L = -1/slope).

The purpose of quantitative EBIC studies of grain boundaries is to determine with high accuracy the recombination velocity at the grain boundary $v_{g.b.}$ and the diffusion length in the grains L. In a general case the simple equation (18) is not sufficient. More complex relations have been obtained by several authors [6,7,25, 64,65,66,80]. The calculation difficulties are due to the complex geometry of the system consisting of two perpendicular planes (the grain boundary with the boundary condition $D(\partial\delta n/\partial z) = v_{g.b.}\delta n$, and the collection plane) and an extended non-homogeneous source. The importance of considering a realistic excitation volume, particularly at small distances x, was discussed in [6,25,65,80]. For Si, only at distances x greater than two excitation-volume radii, an accuracy better than ten percent can be expected for a point-source approximation [6]. Accurate measurements require frequent fitting of experimental and theoretical EBIC responses. An elegant graphical procedure which allows a simultaneous determination of $v_{g.b.}$ and L from the area of the contrast profile

$$A = \int_{-\infty}^{+\infty} c(x)\, dx \qquad (19a)$$

and the variance σ^2 (giving the profile spread)

$$\sigma^2 = \frac{1}{A} \int_{-\infty}^{+\infty} x^2 c(x)\, dx \qquad (19b)$$

was developed by Donolato [25]. Fig. 9 shows Donolato's diagram for the evaluation of $v_{g.b.}$ and L. Since R is known, and A and σ can be derived from the contrast profile, one can determine both $v_{g.b.}$ and L from Fig. 9. By interfacing a microcomputer to the SEM an automatic evaluation of $v_{g.b.}$ and L is possible [26].

Quantitative evaluation of grain boundaries becomes difficult in polycrystalline materials with grain sizes comparable or less than the diffusion length in the singular grains. In such materials EBIC response of a grain boundary is affected by the neighbour boundaries [75,44]. Calculations for two parallel boundaries have shown that the grain boundary with the smaller effective recombination velocity becomes less and less visible the smaller the distance between the boundaries [44]. The EBIC current in such a system depends on the grain size, the diffusion length in the grain, the distance of the generation volume from the grain boundary, the depth of the generation volume, and the grain boundary recombination velocities.

The EBIC contrast profile becomes asymmetric when two adjacent grains have different diffusion lengths [71]. This is illustrated in Fig. 10. The minimum of the EBIC signal is shifted away from the grain boundary toward the region with shorter diffusion length, and it disappears altogether for small surface recombination velocities ($v_{g.b.} < 10^4$ cm/s). Its magnitude differs markedly from those calculated for equal diffusion lengths. These effects become negligible for large recombination velocities at grain boundaries (for p-type silicon this happens for $v_{g.b.} \geq 10^5 cms^{-1}$).

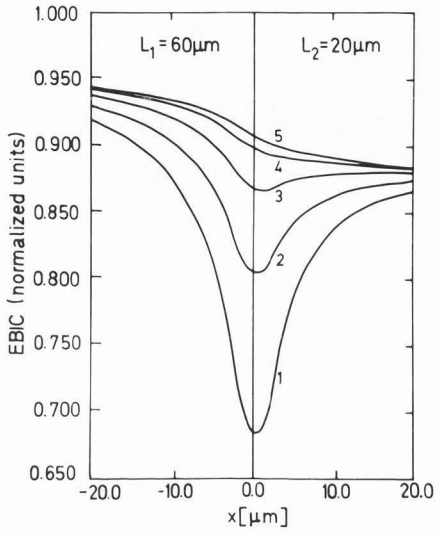

Fig. 10. Normalized EBIC profiles for a semi-infinite grain boundary in Si, normal to the x axis; the adjacent grains have different diffusion lengths (60 μm and 20 μm); curve 1: $v_{g.b.} = 10^5$ cm/s, curve 2: $v_{g.b.} = 3x10^4$ cm/s, curve 3: $v_{g.b.} = 10^4$cm/s, curve 4: $v_{g.b.} = 3x10^3$ cm/s, curve 5: $v_{g.b.} = 10^3$cm/s. The profiles have been calculated for D = 30 cm^2/s and beam energy 30 keV (Fig. 2 in Ref. 71).

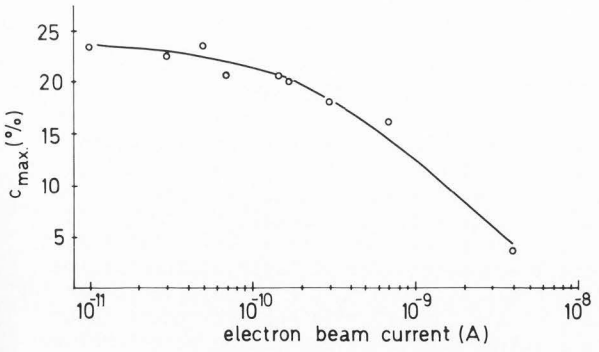

Fig. 11. Maximum contrast versus electron beam current, measured at the grain boundary of a p-type Si bicrystal at beam energy 35 keV (Jakubowicz, unpublished results).

Effective and True Recombination Velocity

The quantity $v_{g.b.}$ is an effective recombination velocity for minority carriers at the edge of the grain boundary space charge region. The "true" value of the recombination velocity at the grain boundary traps, has to take into account the presence of the barrier associated with the grain boundary charge [8,73]. For example, Card and Yang [8] found

$$v_{g.b.} \equiv v_{g.b.}^{eff} = \frac{1}{2} v_{g.b.}^{"true"} e^{\phi/kT} \qquad (20)$$

where ϕ is the barrier height. In general, $v_{g.b.}$ depends on the excitation level, i.e. on the excess carrier density. This is because the capture of minority carriers by the grain boundary traps reduces the net charge at the grain boundary traps, and consequently ϕ. Since the EBIC contrast depends on $v_{g.b.}^{eff}$ one obtains different EBIC contrast profiles at different excitation conditions (accelerating voltage, beam current). Fig. 11 shows the maximum contrast (measured at the grain boundary) as a function of the electron beam current. The contrast reduces at higher excitation levels. From the above it is also clear that $v_{g.b.}^{eff}$ changes with distance x from the grain boundary. This problem was treated in detail by Sundaresan et al. [76]. In order to minimize non-linear effects one should work at excitation levels as low as possible.

The problem of the excitation dependent effective recombination velocity in EBIC experiments concerns dislocations, too. Only recently Wilshaw and Booker [77] presented calculations and experimental results for the dependence of EBIC contrast on the beam current. The contrast decreases with increasing beam current that indicates a decrease of the effective recombination velocity with increasing excitation level.

Detection of Local Interface Defects

In realistic situations interfaces are not perfect. For example, EBIC images of grain boundaries in polycrystalline Si show frequently locally enhanced or reduced brightness. This is due to the presence of dislocation conglomerations, impurity clusters, and structural differences of the grain boundaries. Romanowski [68] recently developed a method which allows to estimate the strength of such defects. The method uses a perturbative treatment. Romanowski assumed the boundary condition at the grain boundary to be of the form $D(\partial\delta n/\partial z) = v_{g.b.}\,\delta n + \Delta v_{g.b.}\,\delta n$, where $\Delta v_{g.b.}$ is a small perturbation of $v_{g.b.}$. He also considered a small defect near the grain boundary represented as a local reduction of the diffusion length L by ΔL. Assuming that $\Delta L/L$ is equal to $\Delta v_{g.b.}/v_{g.b.}$ he has shown that a local defect located close to the grain boundary yields a stronger EBIC contrast than a local variation of the grain boundary recombination velocity.

Detection of Space Charge Regions

This method uses for charge collection the defect's own space charge region [47,48]. Fig. 12 represents schematically the expected EBIC contrast profile of a symmetric grain boundary, when the signal is measured by using two ohmic contacts at the adjacent grains. In this method the

space charge region of the investigated grain boundary is used to separate the electron-hole pairs. Since the electric field directions on both sides of the grain boundary are opposite, the EBIC signal changes its sign, when the electron beam crosses the grain boundary. The signal reaches its maximum when the generation volume lies completely on one side of the boundary. The profile from Fig. 12 loses its symmetry when the

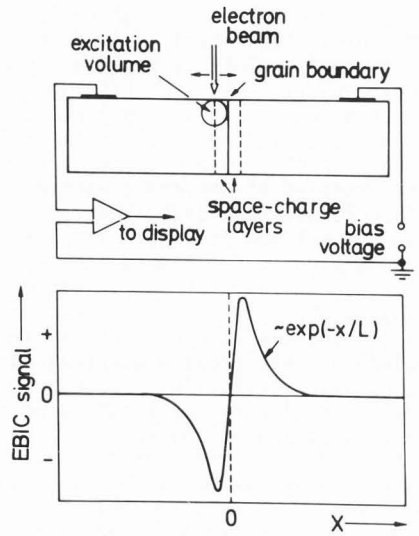

Fig. 12. Schematic circuit for detection of the space charge regions associated with the grain boundary, and the EBIC profile across a symmetric grain boundary (Fig. 1 in Ref. 79).

grain boundary is asymmetric or when a bias voltage is applied. Ziegler et al. [79] discussed the contrast behavior for asymmetric grain boundaries. In their model the grain boundary behaves like two back-to-back Schottky diodes separated by a layer of very small but finite thickness. These Schottky barriers will have different heights when the charges at both sides of the thin layer differ. The authors proposed a method for calculation of the EBIC current across the grain boundary.

Mataré and Laakso [47,48] applied this technique to detect space charges at grain boundaries and isolated dislocations.

Cathodoluminescence Contrast of Localized Defects

In the CL mode of the SEM the image is formed by detecting the light emitted by the sample, which is the product of radiative recombination processes. Since both EBIC and CL imaging are based on local variations of recombination properties of the material and both methods offer a similar spatial resolution (~1 μm), they can be treated as comparable. On the other hand the different signals being measured (current and light, respectively) make them complementary. Whereas the theoretical aspects of EBIC defect imaging have been studied intensively for the last several years, much less attention has been paid to the theory of CL contrast.

The only difference in the geometrical configuration between the EBIC and CL modes is the presence of the Schottky contact in the EBIC mode, which is applied for charge collection. In the case of CL, the total intensity of radiation coming out through the surface is measured, and the surface is characterized by the recombination velocity v_s. If $v_s \approx \infty$, which occurs usually, both geometries become identical. In a linear approach the CL intensity versus electron beam position is given by [43]

$$CL \sim \int_V F_A F_R \eta_{CL}(\vec{r}) \delta n(\vec{r}) dV \qquad (21)$$

where F_A and F_R are correction functions for reabsorption losses inside the material, and reflection losses at the surface, respectively, η_{CL} is the internal quantum efficiency of the material, and V is the volume of the sample.

Recombination processes are characterized by appropriate recombination times. In general, when both radiative and nonradiative recombination occur, the observable recombination time (minority carrier lifetime) is

$$\tau = \frac{\tau_r \tau_n}{\tau_r + \tau_n} \qquad (22)$$

where τ_r and τ_n are the radiative and nonradiative lifetimes, respectively. Assume the material is characterized by a constant optical absorption coefficient α. The CL contrast may be due to two reasons. One originates in spatial variations in τ_r at a practically constant total lifetime. This type of CL contrast occurs when nonradiative processes are dominant in the material, i.e. $\tau_n \ll \tau_r$. Since there is no spatial variation in τ, this situation does not yield a contrast in the EBIC image. The second type of CL contrast is due to variations in τ_n either at a constant value of τ_r, or when $\tau_n \ll \tau_r$. The contrast is then the result of a modified excess carrier distribution due to the presence of the defect.

Löhnert and Kubalek [43] studied CL contrast profiles for localized nonradiative defects regarded as a small perturbation of τ. Their approach is similar to the one of Donolato [16, 18] for the EBIC problem. By numerical calculations for a threading dislocation at right angle to a surface of infinite recombination velocity they found an exponential decay of the CL contrast at sufficient distance from the dislocation with a decay constant of 0.63 minority carrier diffusion lengths. They suggested a method for measuring the minority carrier diffusion length without any electrical contacts to the specimen. They have also shown that the decisive factor for the contrast formation is not the reduction of the quantum efficiency η_{CL} in the defect volume, but the overall reduction of the excess carrier density due to enhanced nonradiative recombination. Taking advantage of this finding Jakubowicz [36] has recently given an analytical solution for the CL contrast profile at sufficient distance from an individual point-like defect,

which takes into account the influence of an arbitrary recombination at the surface and the internal optical absorption. Its general form is

$$c_{CL} = f_1(r_{eff}, v_s, L, H)\, f_2(\alpha, v_s, L, b, h, H) \quad (23)$$

The function f_1 describes the dependence on the defect strength ($r_{eff} \equiv$ capture radius). Since geometrical and material parameters are also involved in f_1, the contrast depends on the capture radius of the defect in a complex manner and is generally a non-linear function of r_{eff}. f_1 can be regarded as an effective defect strength. For weak defects f_1 reduces to

$$f_1 = \frac{r_{eff}}{L}\, e^{r_{eff}/L} \quad (24)$$

and is identical with the appropriate function given by equation (16b) for the EBIC contrast. The function f_2 characterizes the material and the geometry of the system.

Comparison of CL and EBIC Contrasts

In many practical situations the recombination rate at the surface is much higher than in the bulk. On the other hand one has an infinite surface recombination velocity in a standard EBIC geometry with a Schottky contact (see Fig. 1c). Thus, the CL and EBIC modes become complementary methods. For a point-like defect and a point-like source the following relation is valid [36]

$$c_{CL} = c_{EBIC}\, \theta \quad (25)$$

where

$$\theta = \frac{1 - e^{-H(\alpha - \frac{1}{L})}}{1 - e^{-h(\alpha - \frac{1}{L})}} \quad (26)$$

Equation (26) says that in the simple case of a point-like defect and source it depends on their depths, which of both contrasts is larger: $c_{CL} > c_{EBIC}$ if $H > h$, and $c_{CL} < c_{EBIC}$ if $H < h$. There are two cases when both contrasts are equal: (1) $H = h$, (2) $\alpha \gg 1/L$. Equations (25) and (26) suggest a simple method of testing the depth at which the defect is located. If the coefficient of optical absorption, the diffusion length, and the penetration depth of the beam are known one can find the position of the defect by comparing CL and EBIC contrasts at any distance from the defect.

A useful feature of θ is its independence of the defect strength. Thus, as long as $c_{CL}/c_{EBIC} =$ const., any contrast differences at the EBIC or CL micrograph are due to variations of the defect strength. This will hold for extended defects in some cases, too. Assuming for a dislocation parallel to the surface that the main contribution to both CL and EBIC contrasts comes from the part of the dislocation being closest to the source one should be able to reconstruct its "electrical shape". The EBIC and CL contrast magnitudes will change in two cases: (1) when a dislocation segment is at a different depth or (2) when a local variation of the defect strength occurs. Again if $c_{CL}/c_{EBIC} =$ const. a contrast non- uniformity can be attributed to a local variation of recombination properties. This "simple" test may become together with TEM an interesting extension of the CL method for studying decoration effects at dislocations (decoration effects at dislocations can be studied by analysing the changes of the CL spectra of the dislocation and its surrounding) or for detecting differences in the recombination behavior of "clean" dislocations, due to their structural properties.

Numerical calculations for inclined dislocations show that the maxima of CL and EBIC contrasts appear at different positions (Fig. 13).

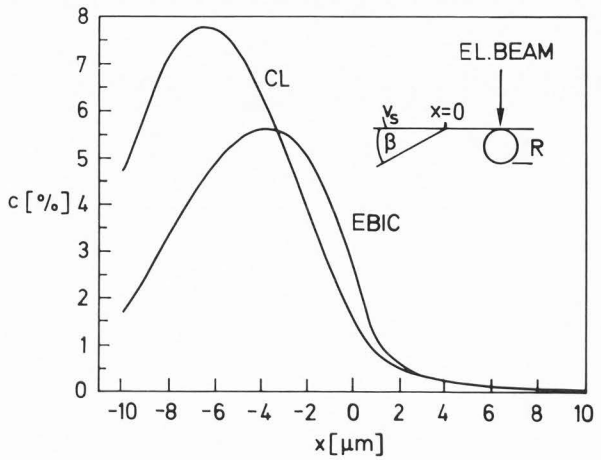

Fig. 13. Calculated CL and EBIC contrast profiles for a straight semi-infinite dislocation lying in the plane $y = 0$ at an angle $\beta = 30°$ to the surface (collecting plane), and intersecting the surface at the center of the coordinate system. The electron beam also moves in the plane $y_2 = 0$. Calculations have been performed for $\alpha = 10^2 cm^{-1}$, $v_s = \infty$, $L = 5$ μm, $R = 5$ μm, $r_{eff} = 100$ Å (Fig. 4c in Ref. 36).

Thus for an observer comparing a CL and EBIC micrograph details may seem to be displaced. This "displacement" depends on the surface recombination velocity and the optical absorption coefficient. A consequence of the latter is that a CL micrograph taken at a singular frequency of emitted radiation may show better resolution than the same micrograph obtained by using the integral CL signal. One should also be careful, when interpreting an experiment performed in conditions with α not being constant.

A theoretical study similar to the above has been performed recently by Pasemann and Hergert [61]. These authors have proposed a CL/EBIC method for the determination of the depth of a lattice defect. As an example they have chosen a dislocation parallel to the surface.

At the moment there is no convincing experimental evidence for the validity of the theoretical findings discussed in this section. However differences between CL and EBIC micrographs were observed. A careful observation of

Fig. 4 in Ref. 11, presenting CL and EBIC pictures from the same area of a GaP layer, reveals significant differences at the individual (corresponding to each other) black spots. There are also preliminary results of a simultaneous CL/EBIC experiment at dislocations in GaAs (presented by Jakubowicz at the Fourteenth International Conference on Defects in Semiconductors, Paris, 1986). These results are consistent with theoretical findings.

In the above considerations it has been assumed that both CL and EBIC contrasts are due to enhanced non-radiative recombination at the defect. The situation complicates when both radiative and non-radiative transitions contribute to the CL contrast. For example, the CL contrast may change opposite to the EBIC contrast if a particular radiative recombination process either appears or vanishes (this is often observed in CL/EBIC versus temperature measurements).

Time-Dependent EBIC and CL Measurements in Presence of Localized Defects

There are at least two reasons to perform time-dependent measurements at localized defects. First, the rise and decay times of EBIC and CL signals after respectively switching on and off the electron beam depend directly on the minority carrier lifetime. Thus, from a time-dependent measurement one obtains immediately the recombination efficiency of the defect [14]

$$\eta = (1 - \frac{\tau_d}{\tau}) \times 100\% \qquad (27)$$

where τ_d is the lifetime measured at the defect, and τ is the bulk lifetime. In DC measurements, lifetimes are deduced from the diffusion lengths by using the relation $L = (D\tau)^{1/2}$, and by assuming D to be known and constant. Second, the possibility of a direct determination of τ_d, provides together with DC measurements a method of determination of D (the diffusion constant D around a defect may differ from its bulk value).

CL time-dependent measurements at individual dislocations and grain boundaries were performed by several authors [74,12,13,51]. The lifetimes associated with individual defects were deduced by comparing CL decays measured far from and at the defects. Romanowski and Wittry [69] used rise-times of the EBIC signal to estimate lifetimes at individual grain boundaries in polycrystalline Si. Only in recent months theoretical studies appeared, which give consideration to the presence of an individual defect. Jakubowicz [33] has given an analytical solution of the EBIC time-dependent problem for a weak point-like defect of capture radius r_{eff}, and point-like source. At sufficient large distances b (Fig. 1c) the EBIC decay after electron beam cut-off can be generally written as

$$EBIC(t) = \text{const.}\,[f(t,\tau,L,h) - f(t,\tau,r_{eff},L,H,h,b)] \qquad (28)$$

or in a more compact form as

$$EBIC(t) = EBIC_b(t) - EBIC_d(t) \qquad (29)$$

where t is the time, and the indices b and d are related to the background current and to the contribution of the defect to the collected current. The current versus time decay shows a complicated non-linear dependence on the geometrical parameters of the system (h,H,b), the bulk properties (τ,L), and the capture radius of the defect.

Fig. 14a illustrates computational results for a single dislocation, regarded as a row of

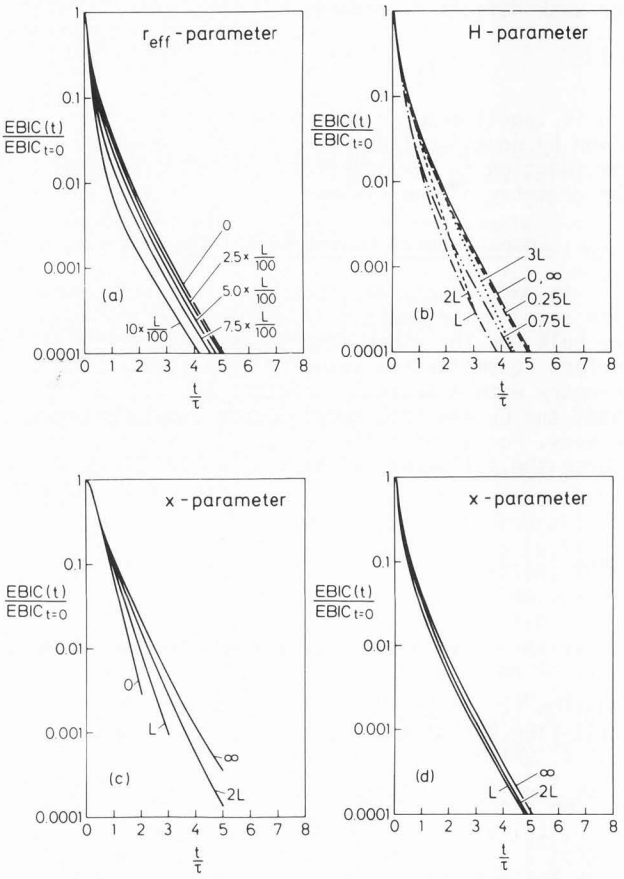

Fig. 14. Plots of EBIC vs normalized time in the presence of a straight dislocation of infinite length, parallel to the collection plane of a semi-infinite sample. (a) The effective radius of the dislocation is the varying parameter. It has been assumed that both the dislocation and the point source are at the same depth H = h = 0.5 L. The distance between the dislocation and the source is equal to one diffusion length (x = L); (b) r_{eff} = 0.05 L, h = 0.5 L, x = L, H is the varying parameter, the symbol "0,∞" means that the same curve is valid for both H=0 and H=∞; (c) r_{eff} = 0.05 L, h = L, H = 2L, x is the varying parameter; (d) r_{eff} = 0.05 L, h = 0.5 L, H = 0.5 L, x is the varying parameter; (a), (b), (c), and (d) correspond to Figs. 5b, 8a, 6a and 6b, respectively, in Ref. 33.

point-like defects, parallel to the surface. The curves show a trend similar to the one observed experimentally in cathodoluminescence studies. Even without any localized defect ($r_{eff} = 0$) there is a rapid initial decay followed by a slower near- exponential one. The rapid initial decay is due to the boundary condition at the collection plane (see Fig. 1c) $\delta n = 0$ ($v_s = \infty$). A similar effect has been predicted theoretically for the CL decay at high surface recombination velocities [5,35].

The effect of the dislocation is a more rapid decay of the current.

A nonmonotonic character of the slope variations is observed at curves calculated for different dislocation depths (Fig. 14b). Notice that the curves in Fig. 14b cross. This effect appears due to the complicated geometry of the system, which makes the current decay nonexponential.

The asymptotic slope (at large times) in Fig. 14b increases with increasing dislocation depth H, reaches a maximum and decreases with further increase of H. As can be expected, one gets the same slope for very small (curve H=0) and very large (curve H=∞) dislocation depths. In both limit cases, one has a situation which corresponds to the absence of any defect (H=0 means the defect belongs to the collecting plane with $v_s=\infty$, and H=∞ means the defect is infinitely far from the collecting plane).

The decay changes provided by a defect, and thus their experimental detectability depend strongly on the set of parameters r_{eff}, H, h, x, and L. This is illustrated in Fig. 14c and d. It may be difficult to detect any changes when the defect is located at a depth much smaller than the diffusion length (Fig. 14d). Measurable changes can be expected at larger defect depths (Fig. 14c). Calculations performed for a constant defect depth and various electron ranges have shown that the decay slope can be maximized by selecting an optimal electron beam accelerating voltage.

The system for decay measurements should be able to detect small signals, since any differences in the initial part of the decay can be below the resolution limit of the method. On the other hand, at very long times one obtains an asymptotic slope which is controlled by the bulk lifetime only (see Figs. 14a and 14d; in Figs. 14b and 14c the curves do not reach the long time regime). It results from the above that one should always find an optimal range in which the slope differences are maximal.

Another limitation of this method may be due to the capacitance C of the collecting Schottky contact or p-n junction, and the series resistance of the sample R_s. The time constant R_sC determines the minimal measurable lifetime. This problem was recently treated in detail by Romanowski et al. [67], who analysed the EBIC decay in the presence of a single grain boundary perpendicular to the surface. Fig. 15 shows EBIC versus time plots for three different values τ/R_sC. The influence of the time constant on the detectability of the grain boundary is evident. Whereas the grain boundary is easily detectable for $\tau/R_sC = 33$, one can hardly distinguish the decays near and far from the grain boundary when $\tau/R_sC = 3.3$.

A new EBIC time-dependent method of quantitative defect evaluation has been developed recently by Romanowski and Wittry (to be published). They analysed the first harmonic of the AC-EBIC signal generated by a gated electron beam near a grain boundary and have shown that one can determine from the first harmonic the diffusion length in the grains, the lifetime, and the grain boundary recombination velocity. The analysis is performed for a point source and square wave generation function. The authors have used this method to evaluate lifetimes in polycrystalline Si.

Final Remarks

Further work on both CL and EBIC imaging of defects is still necessary. All theoretical calculations dealing with EBIC and CL imaging assumed the defect to be a region of enhanced recombination (black dot contrast). However, it is well known that in both modes defects may appear as bright spots. Recently, for example, Hwang et al. [30] suggested that oxygen precipitates attract minority electrons in p-Si, but repel minority holes in n-Si, which is due to the fixed positive oxide charge of the precipitates. Since the precipitates have interface states acting as recombination centers it is clear that in p-Si they will appear as dark spots. In n-Si, if the repelling potential will be large enough one will observe an increase of the EBIC signal when approaching the defect by the beam. A bright spot may be also seen in case of a defect acting as a gettering site for impurities, when the effect of the resulting denuded zone will be stronger than the effect due to recombination at the defect.

Recently Jakubowicz and Habermeier suggested a way of treating theoretically bright and dark

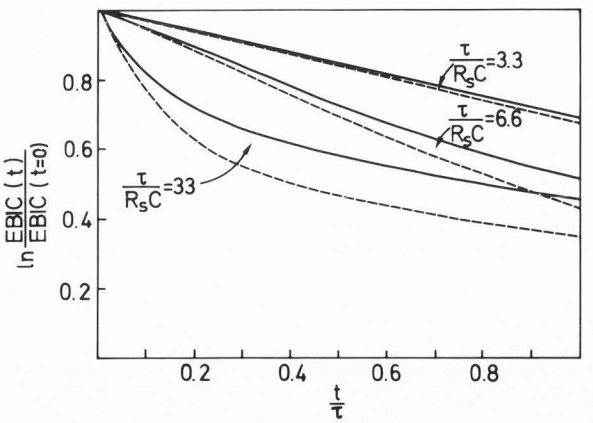

Fig. 15. Plots of ln [EBIC(t)/EBIC(t=0)] vs normalized time in the presence of a semi-infinite grain boundary (in Si) normal to the x axis, for a point source located infinitely far (continuous line) and at a distance x = 3 μm (dashed line) from the grain boundary, calculated for L = 25 μm, $v_{g.b.} x \tau$ = 100 μm and beam energy 30 keV. The varying parameter is τ/R_sC (Fig. 5 in Ref. 67).

contrasts [34]. Preliminary results (Jakubowicz, unpublished) show that bright and dark appearing defects, having equal effective action radii, yield contrast profiles of different half-widths. This means the two types of contrasts may be observed with a different spatial resolution.

The situation may be even more complex in the case of the CL mode. For example, in addition to a reduced total lifetime the defect itself may be luminescent. If this luminescence will be strong enough the defect will appear bright. In Ref. 74 the dislocation appears dark although the total lifetime at the dislocation increases. This is probably due to an increase of the radiative part of the total lifetime at a practically constant nonradiative component. Moreover, bright and dark contributions from the same defect may be spatially resolved, like in the case of "dot and halo" contrast [1]. In both CL and EBIC modes a reversal of the contrast sign has been observed, which depends on the excitation level [34,1]. This phenomenon is not fully understood. In [1] the CL contrast sign reversal has been explained by local heating of the specimen by the electron beam giving rise to a dominance of nonradiative recombination. The sign reversal of the EBIC contrast, observed at oxygen precipitation related defects in Si [34], has been interpreted as a change of the effective recombination velocity at the defect. It is known that the effective recombination velocity depends on the excitation level. Therefore, when the defect has a complex structure (for example an oxygen precipitation related dislocation), it may depend on the excitation level whether the black or white dot contrast prevails.

The majority of theoretical studies concentrated attention mainly on: (a) the geometrical aspects of EBIC and CL contrasts of defects, (b) the evaluation of a global parameter (the defect strength) characterizing the defect recombination activity, and (c) the evaluation of bulk parameters in the presence of defects. It seems to the author that more theoretical work, which gives direct insight into the individual recombination processes, is necessary. Dopant concentration-, temperature-, and time-dependent measurements seem promising for this purpose. The defects should be represented as more realistic objects.

Much more attention should be paid to CL imaging of defects, since this technique becomes more and more attractive for characterization of defects in semiconductor compounds used in optoelectronics. In the CL mode both carrier and photon transport should be studied simultaneously.

Recent applications of transmission electron microscopy and scanning transmission electron microscopy combined with CL require a theoretical treatment of CL contrast in very thin samples. As shown by Pennycook [62] the spatial resolution of CL images depends strongly on the sample thickness, improving with its decrease. However, resolutions obtained experimentally differ from the ones predicted by a former theoretical estimation [62].

Extensive experimental work has been performed on spectral properties of defect luminescence (see for example [63,2,52]). It has been shown, for instance, that different radiative transitions may exhibit different contrast behavior [52]. Theoretical studies in this field could make easier the task of "deciphering" the structure, and electrical and optical properties of individual defects.

List of Symbols

A area of the contrast profile.
b distance between the source and the defect.
c contrast.
c_1 EBIC contrast in first-order approximation.
c_k non-linear EBIC contrast (due to higher order approximations).
c_{EBIC} EBIC contrast.
c_{CL} CL contrast.
C capacitance of the collecting Schottky contact or p-n junction.
D minority carrier diffusion coefficient.
$e_{d,min}$ minimal detectable line density for line-shaped defects.
F_A correction function for reabsorption losses.
F, F_{opt} geometrical factors involved in contrast.
F_R correction function for reflection losses.
g number of generated electron-hole pairs per unit time and volume.
h position of the generation volume.
H depth of the defect.
I diffusion current.
I_0 EBIC signal measured when the beam is located infinitely far from the defect.
$I_d(x,y)$ EBIC signal measured when the beam is located at a distance $(x^2+y^2)^{1/2}$ from the defect.
k the relative error of the first-order approximation EBIC contrast.
ℓ radius of dislocation.
L minority carrier diffusion length.
L_d minority carrier diffusion length inside the defect region.
N_d density of recombination centres.
$n_{d,min}$ minimal detectable number of centres for point-like defects.
P area of the collecting barrier.
p an adjustable parameter for modeling grain boundaries by a function $L(x)$.
q magnitude of electronic charge.
$\bar{r}$ representation of coordinates in three dimensions.
R primary electron range.
r_{eff} effective capture radius.
R_s series resistance of the sample.
t time.
T temperature.
V volume of the sample.
v_s surface recombination velocity.
$v_{g.b.}$ recombination velocity at a grain boundary.
w half-width of a contrast profile.
x,y,z cartesian coordinates.
Y length of dislocation.
z_0 depth of the collecting barrier.
α optical absorption coefficient.
γ recombination strength of a dislocation.
γ_d strength of a defect.
Γ recombination strength of point-like/line defects.
δn density of excess minority carriers.
η recombination efficiency of a defect.

η_{CL} internal quantum efficiency.
$\Theta = c_{CL}/c_{EBIC}$.
v_{th} thermal velocity of minority carriers.
σ^2 variance of the contrast profile.
σ_d capture cross-section of recombination centres.
τ lifetime of minority carriers.
τ_d minority carrier lifetime inside the defect region.
τ_n non-radiative lifetime.
τ_r radiative lifetime.
ϕ grain boundary barrier height.
Φ carrier collection probability.

References

1. Balk LJ, Kubalek E, Menzel E. (1976) Investigations of as-grown Dislocations in GaAs Single Crystals in the SEM. Scanning Electron Microsc. 1976; I: 257-264.

2. Batstone JL, Steeds JW. (1985) TEM and CL Characterization of Dislocations in OMCVD ZnSe. In Microscopy of Semiconducting Materials, Inst. Phys. Conf. Ser. 76 AG Cullis, DB Holt (eds.), Bristol and Boston, 383-388.

3. Beer M, Menniger H, Raidt H, Rohrbeck W. (1980) On the Analysis of EBIC Contrast of Crystal Defects. Phys. Stat. Sol. (a) 61, 365-372.

4. Blumtritt H, Gleichmann R, Heydenreich J, Johansen H. (1979) Combined Scanning (EBIC) and Transmission Electron Microscopic Investigations of Dislocations in Semiconductors. Phys. Stat. Sol. (a) 55, 611-620.

5. Boulou M, Bois D. (1977) Cathodoluminescence Measurements of the Minority-Carrier Lifetime in Semiconductors. J. Appl. Phys. 48, 4713-4721.

6. Burk DE. (1982) The Importance of the Excitation Volume in Determination of Surface Recombination Velocity. IEEE Trans. Electron Devices ED-29, 1887-1896.

7. Burk DE, Kanner S, Muyshondt JE, Shaulis DS, Russell PE. (1983) Determination of Surface Recombination Velocity at a Grain Boundary Using Electron-Beam-Induced Current. J. Appl. Phys. 54, 169-173.

8. Card HC, Yang ES. (1977) Electronic Processes at Grain Boundaries in Polycrystalline Semiconductors under Optical Illumination. IEEE Trans. Electron Devices ED-24, 397-402.

9. Castellani L, Gondi P, Patuelli C, Berti R. (1982) On the EBIC Contrast of Dislocations in Si. Phys. Stat. Sol. (a) 69, 677-685.

10. Cheng LJ. (1984) Recombination-Active Defects in Silicon Ribbon and Polycrystalline Solar Cells. 13th Int. Conf. on Defects in Semiconductors. (Eds.): Kimerling LC, Parsey, Jr. JM. A publication of the Metallurgical Society of AIME, Warrendale, Pennsylvania, 403-409.

11. Darby DB, Booker GR. (1977) Scanning Electron Microscope EBIC and CL Micrographs of Dislocations in GaP. J. Mater. Sci. 12, 1827-1833.

12. Dimitriadis CA, Huang E, Davidson SM. (1978) SEM Cathodoluminescence Studies of Dislocation Recombination in GaP. Solid-St. Electron. 21, 1419-1423.

13. Dimitriadis CA. (1983) Carrier Recombination at Dislocations in Epitaxial Gallium Phosphide Layers. Solid-St. Electron. 26, 633-637.

14. Dimitriadis CA. (1984) Recombination Efficiency of Single Dislocations in GaP. Solid State Communications 49, 1111-1112.

15. Dimitriadis CA. (1985) A Scanning-Electron- or Light-Beam-Induced Current Method for Determination of Grain Boundary Recombination Velocity in Polycrystalline Semiconductors. IEEE Trans. Electron Devices ED-32, 1761-1765.

16. Donolato C. (1978/79) On the Theory of SEM Charge-Collection of Localized Defects in Semiconductors. Optik 52, 19-36.

17. Donolato C. (1979) Spatial Resolution of SEM-EBIC Images. Solid-St. Electron. 22, 797-799.

18. Donolato C. (1979) Contrast and Resolution of SEM Charge-Collection Images of Dislocations. Appl. Phys. Lett. 34, 80-81.

19. Donolato C, Klann H. (1980) Computer Simulation of SEM Electron Beam Induced Current Images of Dislocations and Stacking Faults. J. Appl. Phys. 51, 1624-1633.

20. Donolato C. (1981) An Analytical Model of SEM and STEM Charge Collection Images of Dislocations in Thin Semiconductor Layers. Phys. Stat. Sol. (a) 66, 445-454.

21. Donolato C. (1981) An Analytical Model of SEM and STEM Charge Collection Images of Dislocations in Thin Semiconductor Layers. Phys. Stat. Sol. (a) 65, 649-658.

22. Donolato C. (1981) EBIC Image Profiles of Dislocations in the STEM. Inst. Phys. Conf. Ser. 60, 215-220.

23. Donolato C, Venturi P. (1982) Influence of the Generation Distribution on the Calculated EBIC Contrast of Line Defects. Phys. Stat. Sol. (a) 73, 377-387.

24. Donolato C. (1983) Quantitative Evaluation of the EBIC Contrast of Dislocations. J. Physique Colloq. 44, C4-269 - C4-275.

25. Donolato C. (1983) Theory of Beam Induced

Current Characterization of Grain Boundaries in Polycrystalline Solar Cells. J. Appl. Phys. 54, 1314-1322.

26. Donolato C, Bell RO. (1983) Characterization of Grain Boundaries in Polycrystalline Solar Cells Using a Computerized Electron Beam Induced Current System. Rev. Sci. Instrum. 54, 1005-1008.

27. Donolato C. (1986) On the Temperature Dependence of the EBIC Contrast of Dislocations in Silicon. J. Physique 47, 171-173.

28. Holt DB, Lesniak M. (1985) Recent Developments in Electrical Microcharacterization Using the Charge Collection Mode of the Scanning Electron Microscope. Scanning Electron Microsc. 1985; I: 67-86.

29. Holt DB, Saba FM. (1985) The Cathodoluminescence Mode of the Scanning Electron Microscope: a Powerful Microcharacterization Technique. Scanning Electron Microsc. 1985; III: 1023-1045.

30. Hwang JM, Schroder DK, Goodman AM. (1986) Recombination Lifetime in Oxygen-Precipitated Silicon. IEEE Electr. Device Letters EDL-7, 172-174.

31. Ioannou DE, Davidson SM. (1980) SEM-EBIC Studies of Boron Implanted Silicon. J. Microsc. 118, 337-342.

32. Jakubowicz A. (1985) On the Theory of Electron-Beam- Induced Current Contrast from Pointlike Defects in Semiconductors. J. Appl. Phys. 57, 1194-1199.

33. Jakubowicz A. (1985) Theory of Lifetime Measurement with the Scanning Electron Microscope in a Semiconductor Containing a Localized Defect: Transient Analysis. J. Appl. Phys. 58, 1483-1488.

34. Jakubowicz A, Habermeier H-U. (1985) Electron-Beam-Induced Current Investigations of Oxygen Precipitates in Silicon. J. Appl. Phys. 58, 1407-1409.

35. Jakubowicz A. (1985) Transient Cathodoluminescence of Semiconductors in a Scanning Electron Microscope. J. Appl. Phys. 58, 4354-4359.

36. Jakubowicz A. (1986) Theory of Cathodoluminescence Contrast from Localized Defects in Semiconductors. J. Appl. Phys. 59, 2205-2209.

37. Kanaya K, Okayama S. (1972) Penetration and Energy-Loss Theory of Electrons in Solid Targets. J. Phys. D: Appl. Phys. 5, 43-58.

38. Kimerling LC, Leamy HJ, Patel JR. (1977) The Electrical Properties of Stacking Faults and Precipitates in Heat-Treated Dislocation-Free Czochralski Silicon. Appl. Phys. Lett. 30, 217-219.

39. Kittler M, Seifert W. (1981) On the Sensitivity of the EBIC Technique as Applied to Defect Investigations in Silicon. Phys. Stat. Sol. (a) 66, 573-583.

40. Kittler M, Seifert W. (1981) On the Characterization of Individual Defects in Silicon by EBIC. Cryst. Res. Tech. 16, 157-162.

41. de Kock AJR. (1977) SEM Observation of Dopant Striae in Silicon. J. Appl. Phys. 48, 301-307.

42. Leamy HJ. (1982) Charge Collection Scanning Electron Microscopy. J. Appl. Phys. 53, R51-R80.

43. Löhnert K, Kubalek E. (1984) The Cathodoluminescence Contrast Formation of Localized Non-Radiative Defects in Semiconductors. Phys. Stat. Sol. (a) 83, 307-314.

44. Luke KL, von Roos O. (1984) A Theoretical Study of the Effects of Interacting Grain Boundaries on Electron-Beam-Induced Currents. J. Appl. Phys. 55, 2962-2966.

45. Marek J. (1982) Scanning Electron Microscope Charge-Collection Images of Grain Boundaries. J. Appl. Phys. 53, 1454-1460.

46. Marten HW, Hildebrand O. (1983) Computer Simulation of Electron Beam Induced Current (EBIC) Linescans across pn-Junctions. Scanning Electron Microsc. 1983; III: 1197-1209.

47. Mataré HF, Laakso CW. (1968) Scanning Electron Beam Display of Dislocation Space Charge. Appl. Phys. Lett. 13, 216-218.

48. Mataré HF, Laakso CW. (1969) Space-Charge Domains at Dislocation Sites. J. Appl. Phys. 40, 476-482.

49. Mil'shtein SK, Joy DC, Ferris SD, Kimerling LC. (1984) Defect Characterization Using SEM-CCM; Relative Contrast Measurements. Phys. Stat. Sol. (a) 84, 363-369.

50. Mil'shtein S. (1985) Dislocation Trapping Potential Measured by SEM-CCM. In Microscopic Identification of Electronic Defects in Semiconductors, Materials Research Society 46, ed. by NM Johnson, SG Bishop, GD Watkins, Pittsburgh, Pennsylvania, 487-492.

51. Myhajlenko S, Davidson SM, Hamilton B. (1983) SEM CL Assessment of Minority Carrier Lifetime in Silicon. Inst. Phys. Conf. Ser. 67, 327-332.

52. Myhajlenko S, Batstone JL, Hutchinson HJ, Steeds JW. (1984) Luminescence Studies of Individual Dislocations in II-VI (ZnSe) and III-V (InP) Semiconductors. J. Phys. C: Solid State Phys. 17, 6477-6492.

53. Ourmazd A, Booker GR. (1979) The Electrical Recombination Efficiency of Individual Edge

Dislocations and Stacking Fault Defects in n-Type Silicon. Phys. Stat. Sol. (a) 55, 771-784.

54. Ourmazd A. (1981) A Theoretical Interpretation of the Electrical Behaviour of Individual Edge Dislocations in Si as Determined by Combined EBIC/TEM Studies. Cryst. Res. Tech. 16, 137-146.

55. Ourmazd A, Wilshaw PR, Booker GR. (1983) The Temperature Dependence of EBIC Contrast from Individual Dislocations in Silicon. J. Physique Colloq. 44, C4-289-C4-295.

56. Pasemann L. (1981) A Contribution to the Theory of the EBIC Contrast of Lattice Defects in Semiconductors. Ultramicroscopy 6, 237-250.

57. Pasemann L. (1981) On the EBIC Contrast of Dislocations. Cryst. Res. Tech. 16, 147-148.

58. Pasemann L, Blumtritt H, Gleichmann R. (1982) Interpretation of the EBIC Contrast of Dislocations in Silicon. Phys. Stat. Sol. (a) 70, 197-209.

59. Pasemann L. (1984) Some Remarks on the Review "Quantitative Evaluation of the EBIC Contrast of Dislocations" by C. Donolato. J. Physique-Lettres 45, L-133 - L-136.

60. Pasemann L. (1984) Theoretical Study of the Temperature Dependence of EBIC Contrast from Individual, Surface-Parallel Dislocations in a Schottky Diode. Phys. Stat. Sol. (a) 84, 133-142.

61. Pasemann L, Hergert W. (1986) A Theoretical Study of the Determination of the Depth of a Dislocation by Combined Use of EBIC and CL Technique. Ultramicroscopy 19, 15-22.

62. Pennycook SJ. (1981) Investigation of the Electronic Effects of Dislocations by STEM. Ultramicroscopy 7, 99-104.

63. Petroff PM, Weisbuch C, Dingle R, Gossard AC, Wiegmann W. (1981) Luminescence Properties of GaAs-$Ga_{1-x}Al_xAs$ Double Heterostructures and Multiquantum-Well Superlattices Grown by Molecular Beam Epitaxy. Appl. Phys. Lett. 38, 965-967.

64. Romanowski A, Buczkowski A. (1985) The Measurement of the Diffusion Length and the Recombination Velocity at the Grain Boundary in Polycrystalline Solar Cells by the SEM-EBIC Technique. Solid-St. Electron. 28, 645-652.

65. Romanowski A, Buczkowski A. (1985) The Contrast Characteristics of the Grain Boundary near the Boundary Layer in Polycrystalline Solar Cells. Solid-St. Electron. 28, 1199-1206.

66. Romanowski A, Buczkowski A. (1985) The SEM-EBIC Signals near the Grain Boundary in a Polycrystalline Solar Cell. Solid-St. Electron. 28, 1207-1214.

67. Romanowski A, Wittry DB, Tsaur JM. (1986) Analysis of the Short-Circuit Current of a Polycrystalline Solar Cell with Excitation by a Gated Electron Beam. J. Appl. Phys. 59, 951-957.

68. Romanowski A. (1986) Electron-Beam-Induced Current near the Localized Defects in a Polycrystalline Semiconductor. J. Appl. Phys. 60, 2401-2405.

69. Romanowski A, Wittry DB. (1986) Measurement of Carrier Lifetime, Effective Recombination Velocity, and Diffusion Length near the Grain Boundary Using the Time-Dependent Electron-Beam-Induced Current. J. Appl. Phys. 60, 2910-2913.

70. von Roos O. (1979) Analysis of the Interaction of an Electron Beam with a Solar Cell-III. Solid-St. Electron. 22, 773-778.

71. von Roos O, Luke KL. (1984) Analysis of the Electron- Beam-Induced Current of a Polycrystalline p-n Junction when the Diffusion Lengths of the Material on either Side of a Grain Boundary Differ. J. Appl. Phys. 55, 4275- 4279.

72. van Roosbroeck W. (1955) Injected Current Carrier Transport in a Semi-Infinite Semiconductor and the Determination of Lifetimes and Surface Recombination Velocities. J. Appl. Phys. 26, 380-391.

73. Seager CH. (1981) Grain Boundary Recombination: Theory and Experiment in Silicon. J. Appl. Phys. 52, 3960-3968.

74. Steckenborn A, Münzel H, Bimberg D. (1981) Cathodoluminescence Lifetime Pattern of GaAs Surfaces around Dislocations. J. Lumin. 24/25, 351-354.

75. Sundaresan R, Burk DE. (1984) Diffusion Length and Grain-Boundary Recombination Velocity Measurements with the Scanning Electron Microscope in a Finite Polysilicon Grain. Solid-St. Electron. 27, 177-185.

76. Sundaresan R, Fossum JG, Burk DE. (1984) Demonstration of Excitation-Dependent Grain-Boundary Recombination Velocity in Polycrystalline Silicon. J. Appl. Phys. 56, 964-970.

77. Wilshaw PR, Booker GR. (1985) New Results and an Interpretation for SEM EBIC Contrast Arising from Individual Dislocations in Silicon. In Microscopy of Semiconducting Materials, Inst. Phys. Conf. Ser. 76 AG Cullis, DB Holt (eds.), Bristol and Boston, 329-336.

78. Yacobi BG, Holt DB. (1986) Cathodoluminescence Scanning Electron Microscopy of Semiconductors. J. Appl. Phys. 59, R1-R24.

79. Ziegler E, Siegel W, Blumtritt H, Breitenstein O. (1982) Electrical and EBIC Investigations of GaP Grain Boundaries. Phys. Stat. Sol. (a) 72, 593-605.

80. Zook JD. (1983) Theory of Beam-Induced Currents in Semiconductors. Appl. Phys. Lett. 42, 602-604.

Discussion with Reviewers

S. Myhajlenko: The recent use of STEM/TEM EBIC and CL in defect studies of II-VI and III-V semiconductors has produced some improvement in spatial resolution, typically 100 nanometers. The theory of EBIC/CL defect contrast in very thin samples suitable for TEM analysis has yet to be properly explored. We expect the resolution to be limited by the Debye screening length. This limit should also apply to low voltage SEM applications and therefore will be relevant to some of the theoretical treatments described. What are your comments on the contribution the Debye tail would have on the contrast behaviour as a function of temperature in this matter?
Author: In a system in which the diffusion length and generation volume are not the limiting factors for the resolution, the latter will be determined by a characteristic screening length which depends on the concentration of free carriers and the density of charge in fixed positions (ionized atoms, trapped carriers). Since both the fixed charge and the density of free carriers depend on the Fermi energy, one may expect a rather complex temperature behavior of the screening length, and consequently of the temperature dependence of the resolution. A quantitative estimation of this dependence would require solving the Poisson's equation for all charges present in the system. The effect may be in some cases considerable. For example, Manifacier and Henisch [J. Phys. Chem. Solids 41, 1285 (1980)] showed that one may have to do with an effective screening length differing significantly from the Debye length, if traps are added to a material. It therefore seems that an improvement of the resolution by temperature variation is possible.

Reviewer I: You mention that the EBIC spatial resolution is limited by the defect depth or extension of the generation volume. Could you comment on factors influencing CL spatial resolution in the vicinity of a defect?
Author: The spatial resolution of EBIC and CL depends on the defect depth and extension of the generation volume. In a system in which these factors do not limit the resolution i.e. the appropriate parameters are small enough) three other factors become important: the diffusion length, the probe diameter, and the screening length (Debye tail). In the CL mode the resolution problem is, however, more complex. As discussed in the paper, a CL micrograph taken at a singular frequency of radiation may show better resolution than the same micrograph obtained by using the integral CL signal, if the optical absorption coefficient is a function of frequency. A similar effect will appear, if individual frequencies of defect luminescence can be attributed to different geometrical parts of the defect (for example to the core and Cottrell atmosphere of a dislocation, respectively). Some other factors connected with photon transport may also be of importance. Assume, for example, the defect to be a region of enhanced absorption for light produced outside the defect. The spatial resolution of such CL contrast may depend for example on the critical angle of total reflection at the surface, the quality of the surface, and the thickness of the sample. In thin samples the resolution may be affected by optical interference effects.

C. Donolato: The results of Ref. 55 on the temperature dependence of the EBIC contrast of dislocations are interpreted as supporting the Author's nonlinear model. Please comment on the alternative explanation of those results given in Ref. 27 (J. Physique 47, 171 (1986)).
Author: The arguments presented in Ref. 27 require the existence of a non-separable function $\gamma(\lambda,T)$, i.e. it should be

$$\gamma(\lambda,T) \neq \gamma_1(\lambda)\ \gamma_2(T)\ . \qquad (A)$$

However, if γ is separable one obtains

$$\frac{c_i(T)}{c_i(T_0)} = \frac{\gamma_1(\lambda_i)\ \gamma_2(T)}{\gamma_1(\lambda_i)\ \gamma_2(T_0)}\ , \qquad (B)$$

that means the factor $\gamma_1(\lambda_i)$ cancels, and the normalized contrast becomes independent of the index i. In other words, the explanation presented in Ref. 27 is adequate only if the condition (A) is fulfilled. In a recent theory [77] it has been shown that in general one has

$$\gamma = \gamma_1(\lambda)\ T\ f(\lambda,T)\ . \qquad (C)$$

This result supports the arguments given in Ref. 27. On the other hand, the authors of Ref. 77 claim that in the temperature range of interest (where the contrast is a linear function of the temperature) equation (C) can be approximated with a good accuracy by a function

$$\gamma = \gamma_1(\lambda)\ T\ . \qquad (D)$$

If this approximation is applicable then in the light of the new theory the explanation given in Ref. 27 fails.

D. Köhler: The collecting barrier is usually represented by a plane of infinite recombination velocity. What do you think about the validity of this approximation and have any attempts been made to solve a modified field-dependent continuity equation?
Author: Representing the collecting barrier by a plane of infinite recombination velocity is a good approximation as long as carriers are swept out of the depleted region with a velocity much higher than the diffusion velocity in the neutral bulk of the material (i.e. as long as the demand of the collecting barrier for carriers is much higher than the offer by the neutral bulk). Such an approximation is justified for excitation sites not too close to the depleted region, and under low excitation and short-circuit conditions. There have been made calculations of the field-dependent problem (see [46]), yet to my knowledge no successful theory has been published, which takes into account the presence of a local defect such as for example a dislocation.

An attempt in this direction are the works of Mil'shtein [50] and Mil'shtein et al. [49].

C. Donolato: In the introductory section it is stated that only defects located outside the depletion layer will be considered. However, it often occurs in practice that a defect (e.g. a dislocation or a stacking fault) lies, at least in part, in the depletion layer of the device being investigated. Which modifications of the EBIC contrast theory are required to include this case?
Author: In a general case the electric field-dependent problem should be solved (see also discussion with D. Köhler). In many practical situations, however, reasonable corrections may be sufficient.

G. Koschek: Which modifications of your theory would be necessary to explain bright contrasts in CL or EBIC imaging of defects also theoretically?
Author: In my theory the defect is described by an effective capture radius, and consequently it appears as a dark spot in the EBIC image. It also appears dark in the CL mode if non-radiative transitions are dominating in contrast formation. To transfer this theory to bright contrasts it is enough to assume the defect to be characterized by an appropriate effective "repulsion radius". This can be done for both EBIC and CL if the contrast is either due to locally reduced recombination or due to the presence of a local potential repulsive for minority carriers.

S. Myhajlenko: Some recent theoretical studies discuss the merits of combined EBIC and CL defect contrast measurements, for example, L. Pasemann and W. Herget, Ultramicr. vol. 19, p. 15 (1986). In general, the experimental excitation requirements for the two modes can differ by orders of magnitude. This may invalidate some of the initial assumptions. Any comments?
Author: To compare EBIC and CL contrasts one should measure both contrasts at the same excitation level. The fact that the experimental excitation requirements for EBIC and CL can differ by orders of magnitude does not exclude the possibility of satisfying that condition. Nothing hinders one from measuring EBIC signals at an excitation level which is high enough to get also a detectable CL signal. There is only a danger that for both signals the low excitation conditions will not be satisfied. On the other hand, however, there are practical situations in which detectable CL signals occur at not too high carrier injection levels. By using a large area silicon solid-state detector mounted in the SEM specimen chamber above the sample I could measure rather easily CL contrasts from dislocations in GaAs at a beam current $I_b \approx 10^{-9}$ A and accelerating voltage U≈25-30 kV (I did not check the lower limit of excitation conditions sufficient for making the CL detectable).

S. Myhajlenko: In light of recent advances in the theory of CL defect contrast, what progress does the author anticipate with the general task of CL quantification? In particular, in the direction analogous to quantitative X-ray microanalysis. This would be beneficial for semiconductors given the detection sensitivity of 'optically active' impurities by CL is many orders of magnitude better than by X-rays.
Author: This is a difficult question. Defects can be complex objects, surrounded by electrostatic potential barriers, with different mechanisms involved in recombination. They can have various geometrical shapes. All this complicates the analysis of the contrast, since each defect represents a local boundary condition for the excess carrier transport problem. In addition such parameters as temperature and excitation level may affect the properties of the defect and its surrounding. Another difficulty results from the strongly non-linear dependence of the absorption coefficient on the wave length of radiation. The effect of reabsorbed recombination radiation, and reflection at front and back surfaces should also be considered. Therefore I see some problems in making CL a routine quantitative technique. All these problems are a challenge to theoreticians and experimentalists. The theory of CL defect contrast is in my opinion still at an initial stage.

Reviewer I: Correlation of bright or dark dots with individual dislocations is relatively straightforward using TEM CL. Could you comment on the relative merits of TEM CL and SEM CL for obtaining an understanding of defect recombination mechanisms?
Author: Both techniques have advantages and disadvantages. Let me comment on a few important points. The most attractive features of TEM CL are: the possibility of correlating directly the recombination properties of an individual defect with its type and structure, and in most cases a much better spatial resolution compared to SEM CL. On the other hand, in contrast with SEM CL, TEM CL is a destructive method, requires preparation of samples, and is in many cases much more difficult for interpretation (the effect of the specimen thickness, strong influence of surface recombination, flatness of the specimen, optical interference effects, overlap of electrical fields associated with defects and near-surface regions). An attractive feature of SEM CL is the possibility to correlate easily CL with EBIC (such a correlation by using TEM CL requires much more skill).

G. Koschek: In section "Effective and true recombination velocity" it is mentioned that nonlinear effects can be minimized by low excitation. Please give an example to illustrate this statement.
Author: The problem of non-linear effects due to excitation dependent effective recombination velocities at grain boundaries is discussed in detail in Ref. 76. As illustration of this problem the authors have presented results for unpassivated and passivated grain boundaries in Wacker polycrystalline silicon.